A Parameterized Linear 3D Magnetic Equivalent Circuit for Analysis and Design of Radial Flux Magnetic Gears–Part II: Evaluation

Matthew Johnson, *Member, IEEE*, Matthew C. Gardner, *Member, IEEE*, Hamid A. Toliyat, *Fellow, IEEE*

***Abstract*—This is Part II of a two-part paper on the extension of a previously developed parameterized linear 2D magnetic equivalent circuit (MEC) for radial flux magnetic gears with surface permanent magnets to a 3D model. Part I explains the implementation of the 3D MEC. This section, Part II, evaluates the 3D MEC model's accuracy relative to 2D and 3D nonlinear finite element analysis (FEA) models. First, analysis of three base designs illustrates the impacts of the axial discretization parameters and stack length. This leads to the development of guidelines for selecting the axial discretization parameters. Additionally, the MEC is shown to accurately match 3D FEA in predicting the axial variation of flux densities. Finally, 3D MEC, 2D FEA, and 3D FEA models are deployed for a 144,000 case parametric study. The 2D FEA model significantly overpredicts the torques of designs with short stack lengths. However, the 3D MEC provides a much better agreement with 3D FEA, with less than 1% average absolute discrepancy. Additionally, the 3D MEC model is much faster than the 3D FEA model, with average 3D MEC model evaluation speeds ranging from about 100 times to 300 times faster than the 3D FEA for the base designs.**

***Index Terms*--end effects, finite element analysis, magnetic equivalent circuit, magnetic gear, optimization, permeance network, radial flux, reluctance network, torque density.**

I. Introduction

MAGNETIC gears, like mechanical gears, transform mechanical power between high-speed, low-torque rotation and low-speed, high-torque rotation. However, the noncontact operation of magnetic gears provides many potential advantages over mechanical gears, including inherent overload protection, reduced acoustic noise, reduced maintenance requirements, improved reliability, and physical isolation between shafts. Nonetheless, for magnetic gears to achieve parity with mechanical gears in size and weight, fast and accurate analysis tools must be available for application specific optimizations.

One challenge for the optimization of magnetic gears is that end effects are often more significant than in conventional machines. Thus, 3D simulations and prototypes often yield significantly lower slip torques than the values predicted by 2D evaluations [1]-[6]. In some cases, end effects can alter the optimal values of design parameters such as outer radius, pole counts, and magnet thicknesses [7]. However, many analytical field solutions do not account for end effects, and, while 3D finite element analysis (FEA) can be very accurate, it is generally relatively slow. Thus, a 3D magnetic equivalent circuit (MEC) based approach may yield a beneficial compromise between evaluation speed and accuracy.

Part I of this two-part paper explains the implementation of a 3D extension of the 2D MEC previously presented by the authors in [8] and [9]. The MEC evaluated in this study assumes that the back irons and modulators behave linearly with a constant permeability, as in [9]. Nonetheless, this approach could be extended to model nonlinear materials. This section, Part II, provides a detailed evaluation of the linear 3D MEC model's performance in comparison to nonlinear 3D FEA and nonlinear 2D FEA models. Three base designs are used to develop parameters to control the model's discretization. These parameters are then employed in a 144,000 case optimization study to illustrate the extent of the 3D MEC model's accuracy.

II. Impact of Axial Discretization

The 3D MEC radial flux magnetic gear model developed in Part I of this two-part paper extends the 2D MEC radial flux magnetic gear model implemented in [8] and evaluated in [9] to account for axial flux paths. In order to accomplish this, the 3D MEC implementation introduced 2 new discretization parameters, the number of axial layers in the gear, N_{LIG}, and the number of axial layers outside of the gear, N_{LOG}. Because there is more axial leakage flux in the space near the axial ends of the gear than there is in the axial middle of the gear or the out-of-gear regions further removed from the gear, the axial ends of the gear and the portions of the out-of-gear region just beyond the axial ends of the gear require the most axial resolution. In light of this consideration, rather than

This work was supported in part by the U.S. Army Research Laboratory and was accomplished under Cooperative Research and Development Agreement# 14-10. The views and conclusions contained in this document are those of the authors and should not be interpreted as representing the official policies, either expressed or implied, of the Army Research Laboratory or the U.S. Government. The U.S. Government is authorized to reproduce and distribute reprints for Government purposes notwithstanding any copyright notation herein.

M. Johnson is with the US Army Research Laboratory, College Station, TX 77843 USA (e-mail: matthew.c.johnson186.civ@mail.mil).

M. C. Gardner is with the Electric Powertrains Lab at the University of Texas at Dallas, Richardson, TX 75080 USA (e-mail: Matthew.Gardner@utdallas.edu).

H. A. Toliyat is with the Advanced Electric Machines and Power Electronics Lab at Texas A&M University, College Station, TX 77843 USA (e-mail: toliyat@tamu.edu).

simply using uniform height axial layers throughout the active gear stack and the out-of-gear region, this analysis develops and employs the axial layer height distributions described by

$$\overline{h}_{IG,m} = \frac{\left(N_{LIG}-(m-1)\right)^{k_{z,IG}}}{\sum_{m=1}^{N_{LIG}} m^{k_{z,IG}}} \quad (1)$$

$$h_{IG,m} = \overline{h}_{IG,m} h_{IG}. \quad (2)$$

The expression in (1) gives the normalized height of the m^{th} in-gear axial layer, $\overline{h}_{IG,m}$, as a function of the total number of in-gear axial layers, N_{LIG}, and the in-gear axial layer distribution factor, $k_{z,IG}$. Since this analysis uses a symmetrical half stack gear model, the first in-gear axial layer (m = 1) corresponds to the bottom of the half stack model, which is axially adjacent to the middle of the full gear. Layer index $m = N_{LIG}$ corresponds to the in-gear axial layer at the end of the gear stack, which is axially adjacent to the out-of-gear region. The normalized height of the m^{th} in-gear axial layer, $\overline{h}_{IG,m}$, indicates the fraction of the MEC model's total in-gear region axial height, h_{IG}, that corresponds to the m^{th} in-gear axial layer. As this analysis uses a half stack model, the total in-gear region axial height, h_{IG}, is only half of the actual full magnetic gear stack height. The actual height of the m^{th} in-gear axial layer, $h_{IG,m}$, is then given by (2). Thus, the in-gear axial layer distribution is controlled by 2 scalar parameters, N_{LIG} and $k_{z,IG}$. Setting, $k_{z,IG}$.= 0 yields a uniform axial layer height distribution, with each axial layer having the same axial height. Setting $k_{z,IG} > 0$ results in a non-uniform distribution, with the first in-gear axial layer having the largest axial layer height (the coarsest axial resolution) and the last in-gear axial layer having the smallest axial layer height (the finest axial resolution). Increasing the value of $k_{z,IG}$ produces an increasingly aggressive and imbalanced in-gear axial layer distribution with finer resolution at the gear's axial end and coarser resolution in the gear's axial middle.

The analogous expressions in

$$\overline{h}_{OG,n} = \frac{n^{k_{z,OG}}}{\sum_{m=1}^{N_{LIG}} n^{k_{z,OG}}} \quad (3)$$

$$h_{OG,n} = \overline{h}_{OG,n} h_{OG} \quad (4)$$

define the normalized axial height of the n^{th} out-of-gear axial layer, $\overline{h}_{OG,n}$, as a function of the total number of out-of-gear axial layers, N_{LOG}, and the out-of-gear axial layer distribution factor, $k_{z,OG}$. For all MEC and FEA models used in this study, the total axial height of the out-of-gear region, h_{OG}, was set equal to double the full stack magnetic gear axial height. It is worth noting that this is an overly simplified approach to scaling the axial height of the out-of-gear region, and a more efficient tactic would likely involve determining this height as a function of relevant gear geometry parameters, such as the high speed rotor (HSR) and low speed rotor (LSR) permanent magnet pole arcs and the effective air gap sizes. The first out-of-gear axial layer (n = 1) corresponds to the portion of the out-of-gear region immediately adjacent to the end of the active gear stack. Out-of-gear axial layer index $n = N_{LOG}$ corresponds to the out-of-gear axial layer furthest away from the gear stack. The normalized height of the n^{th} out-of-gear axial layer, $\overline{h}_{OG,n}$, denotes the fraction of the total out-of-gear region axial height, h_{OG}, that corresponds to the n^{th} out-of-gear axial layer. The actual height of the n^{th} out-of-gear axial layer, $h_{OG,n}$, is then given by (4). Thus, much like the in-gear axial layer distribution, the out-of-gear axial layer distribution is also controlled by 2 scalar parameters, N_{LOG} and $k_{z,OG}$. Setting, $k_{z,OG} = 0$ yields a uniform axial layer height distribution, with each out-of-gear axial layer having the same axial height. Setting $k_{z,OG} > 0$ results in a non-uniform distribution, with the first out-of-gear axial layer having the smallest axial height (finest axial resolution) and the last out-of-gear axial layer having the largest axial layer height (coarsest axial resolution). Increasing $k_{z,OG}$ produces a more aggressive and imbalanced out-of-gear axial layer distribution with finer axial resolution at the end of the out-of-gear region closest to the end of the gear stack and coarser axial resolution at the end of the out-of-gear region furthest away from the gear stack.

In order to examine the impact of these axial discretization parameters, the same three base designs used in the evaluation of the 2D MEC model [9] and summarized in Table I were analyzed at axial stack lengths of 30 mm, 100 mm, and 300 mm with both the 3D MEC model and a 3D FEA model. Both models use NdFeB N42 permanent magnets (PMs). For the MEC, the back irons and modulators are assumed to have a relative permeability of μ_r = 3000, as in [9]. The FEA model employs the nonlinear B-H curve for M47 electrical steel for the back irons and modulators. For all 3D MEC evaluations, the cross-sectional MEC discretization parameters were fixed at the values indicated in Table II, which correspond to the coarse mesh settings in [9]. As in [9], the primary metric used to compare the models is the torque on the outer permanent magnet LSR. First, the effects of the in-gear axial discretization parameters, N_{LIG} and $k_{z,IG}$, were characterized by sweeping these variables through the 77 combinations of values specified in the first column of Table III for each of the three base designs at each of the three previously listed axial stack lengths. As indicated in Table III, the out-of-gear discretization parameters, N_{LOG} and $k_{z,OG}$, were fixed at values of 4 and 0, respectively, for these simulations. The effects of the out-of-gear axial discretization parameters, N_{LOG} and $k_{z,OG}$, were also independently characterized by sweeping these variables through the 77 combinations of values specified in the second column of Table III for each of the three base designs at each of the three previously mentioned axial stack lengths. As indicated in Table III, the in-gear discretization parameters, N_{LIG} and $k_{z,IG}$, were fixed at values of 4 and 0, respectively, for these simulations.

The graphs in Figs. 1 and 2 illustrate the results of the in-gear and out-of-gear axial layer discretization parameter sweeps for the 30 mm, 100 mm, and 300 mm stack length designs. Note the vertical axis scaling when analyzing these graphs, as the limited impact of certain discretization parameters results in some very narrow vertical axis ranges for maximum resolution. These graphs indicate that the out-of-gear axial layers distribution plays a more important role in the model's accuracy than the in-gear axial layers distribution.

This behavior is likely a result of the nature of the axial leakage flux paths. The in-gear axial leakage flux primarily travels through the highly permeable modulators and back irons, so these portions of the axial leakage flux paths constitute relatively small parts of the overall axial leakage flux path reluctances. Thus, the in-gear axial resolution has a smaller impact on the overall characterization of the axial leakage flux. However, the out-of-gear axial leakage flux paths travel entirely through nonmagnetic material, so these

TABLE I
Magnetic Gear Base Designs for MEC Model Evaluation

Parameter	Description	Base Design 1	Base Design 2	Base Design 3	Units
P_{HS}	HSR pole pairs	11	4	6	
P_{LS}	LSR pole pairs	45	34	98	
Q_{Mods}	Number of modulators	56	38	104	
R_{Out}	Gear active outer radius	150	175	200	mm
T_{HSBI}	HSR back iron thickness	20	35	40	mm
T_{HSPM}	HSR magnet thickness	9	5	13	mm
T_{HSAG}	HSR air gap thickness	0.5	2	1	mm
T_{Mods}	Modulator thickness	11	17	14	mm
T_{LSAG}	LSR air gap thickness	0.5	2	1	mm
T_{LSPM}	LSR magnet thickness	7	5	7	mm
T_{LSBI}	LSR back iron thickness	20	30	25	mm

TABLE II
Cross-Sectional MEC Discretization Settings

Parameter	Description	Value
ALM	Angular layers multiplier	10
$N_{RL,HSBI}$	Number of radial layers in the HSR back iron	3
RLM_{HSPM}	HSR magnets radial layers multiplier	10
RLM_{HSAG}	HSR air gap radial layers multiplier	10
RLM_{Mods}	Modulators radial layers multiplier	10
RLM_{LSAG}	LSR air gap radial layers multiplier	10
RLM_{LSPM}	LSR magnets radial layers multiplier	10
$N_{RL,LSBI}$	Number of radial layers in the LSR back iron	3
$N_{RL,HSPM,min}$	Minimum number of radial layers in the HSR magnets	3
$N_{RL,HSAG,min}$	Minimum number of radial layers in the HSR air gap	3
$N_{RL,Mods,min}$	Minimum number of radial layers in the modulators	3
$N_{RL,LSAG,min}$	Minimum number of radial layers in the LSR air gap	3
$N_{RL,LSPM,min}$	Minimum number of radial layers in the LSR magnets	3

TABLE III
Axial Layer Discretization Parameter Sweep Definitions

Parameter	In-Gear Axial Layer Discretization Sweep Values	Out-Of-Gear Axial Layer Discretization Sweep Values
N_{LIG}	2, 3, 4, … 12	4
$k_{z,IG}$	0, 0.5, 1, … 3	0
N_{LOG}	4	2, 3, 4, … 12
$k_{z,OG}$	0	0, 0.5, 1, … 3

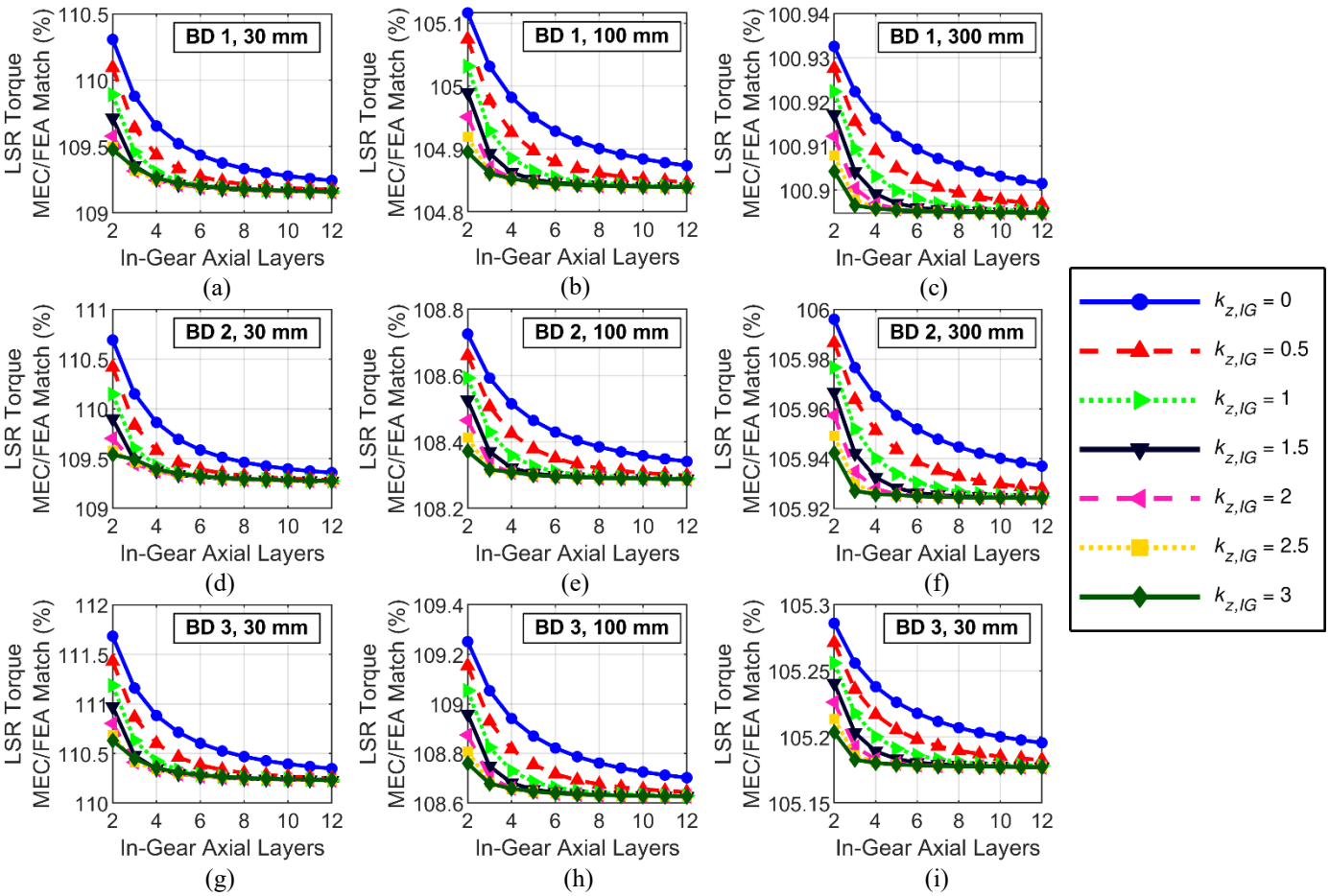

Fig. 1. Variation of radial flux magnetic gear 3D MEC accuracy for Base Designs 1, 2, and 3 at stack lengths of 30 mm, 100 mm, and 300 mm with in-gear axial discretization parameters. Note the difference in the vertical axis scaling between graphs.

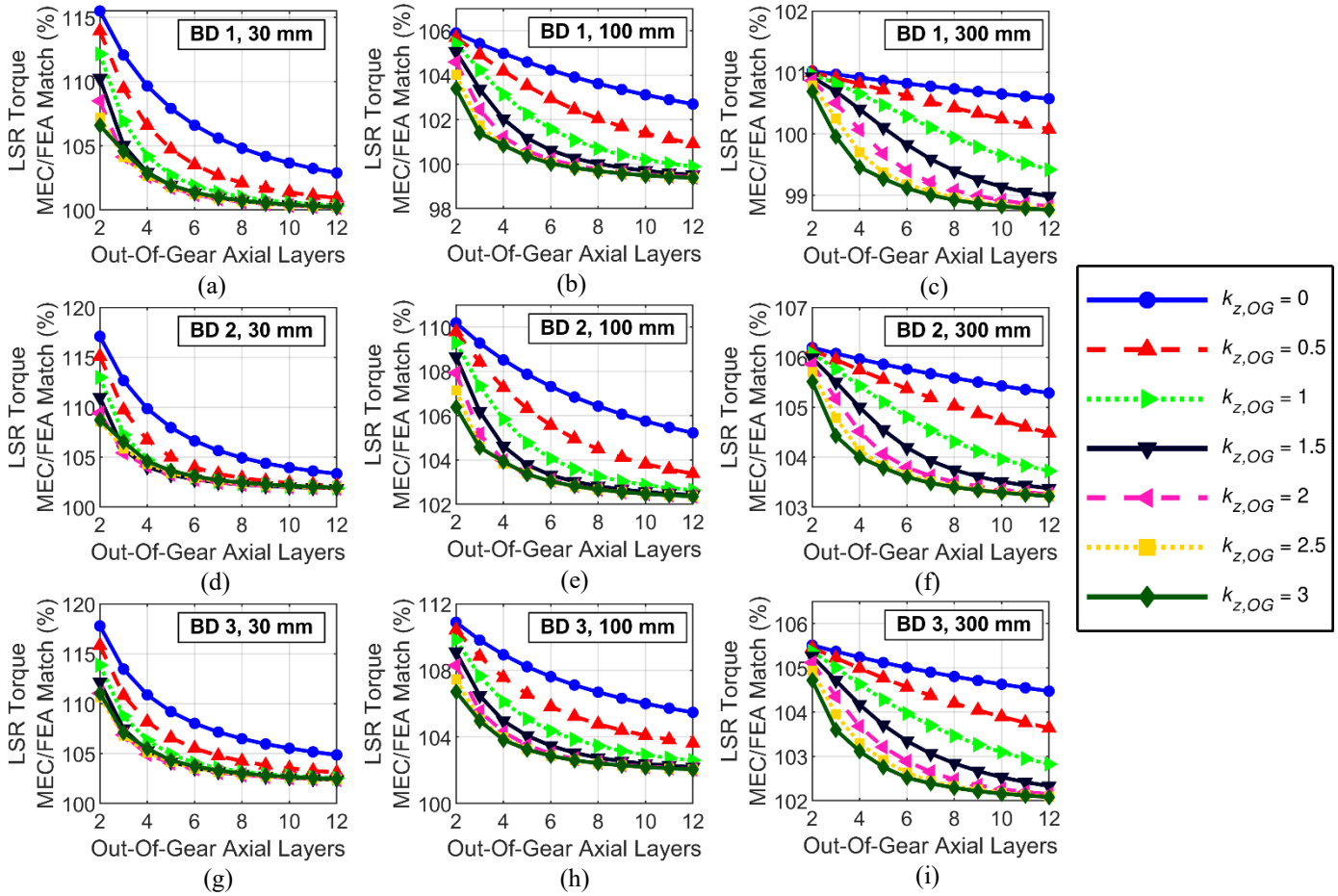

Fig. 2. Variation of radial flux magnetic gear 3D MEC accuracy for Base Designs 1, 2, and 3 at stack lengths of 30 mm, 100 mm, and 300 mm with out-of-gear axial discretization parameters. Note the difference in the vertical axis scaling between graphs.

portions of the axial leakage flux paths account for most of the overall path reluctances, and there is significant variation in the axial leakage flux along these sections of the paths. Thus, the out-of-gear axial resolution has a much more dramatic effect on the overall characterization of the axial leakage flux.

The results in Figs. 1 and 2 also demonstrate that increasing the axial resolution has a more significant effect on the MEC model's accuracy for designs with shorter axial stack lengths. This is not surprising given that 3D effects are simply more impactful for magnetic gears with shorter stack lengths. Gears with long stack lengths generally only experience appreciable axial leakage flux near the ends of the axial stacks, thus these 3D effects have a limited impact on torque transmission capabilities and their accurate characterization (via increased axial resolution) plays a less significant role in the fidelity of the overall design characterization. Consequently, gears with longer stack lengths generally require less axial resolution to accurately determine the slip torque. This also reinforces the commonly accepted notion that if a gear's axial stack length is large enough relative to other key geometric parameters, a 2D model may provide an adequate representation of the design.

Finally, the trends in Figs. 1 and 2 illustrate that increasing the axial layer distribution factors notably improves the model's accuracy, but with diminishing returns. This pattern occurs because increasing the distribution factors produces smaller axial layers near the end of the active gear stack, both in the gear and in the out-of-gear region next to the end of the gear, but it also produces larger axial layers near the middle of the gear stack (at the bottom of the half stack model) and in the part of the out-of-gear region furthest away from the gear. Increasing the distribution factors too much can cause the lack of resolution in the large range of space associated with the axially thick layers to outweigh the high resolution in the limited, but important range of space associated with the axially thin layers. For excessively large distribution factors, this can even negatively affect the model's accuracy. Once the model includes adequate axial layers, there is minimal variation in impact at the high end of the considered axial distribution factor spectrum. The exact effects of the distribution factors and axial layer counts vary for the different base designs and stack lengths, which suggests the need for a future study to develop a more normalized approach to controlling the axial resolution, similar to the angular and radial layers multipliers devised during the analysis of the 2D MEC model [9]. However, the axial layer distribution factors clearly provide a simple, effective, and flexible means of efficiently distributing the axial layers in the 3D MEC model. Additionally, the accuracy of the 3D MEC model could be further improved by using higher resolution 2D discretization settings, but this moderate performance gain would come at the expense of slower simulation times.

III. Flux Density Comparisons

The previous section evaluated the MEC based on the accuracy of its torque predictions relative to those of a nonlinear 3D FEA model. The graphs in Fig. 3 in this section

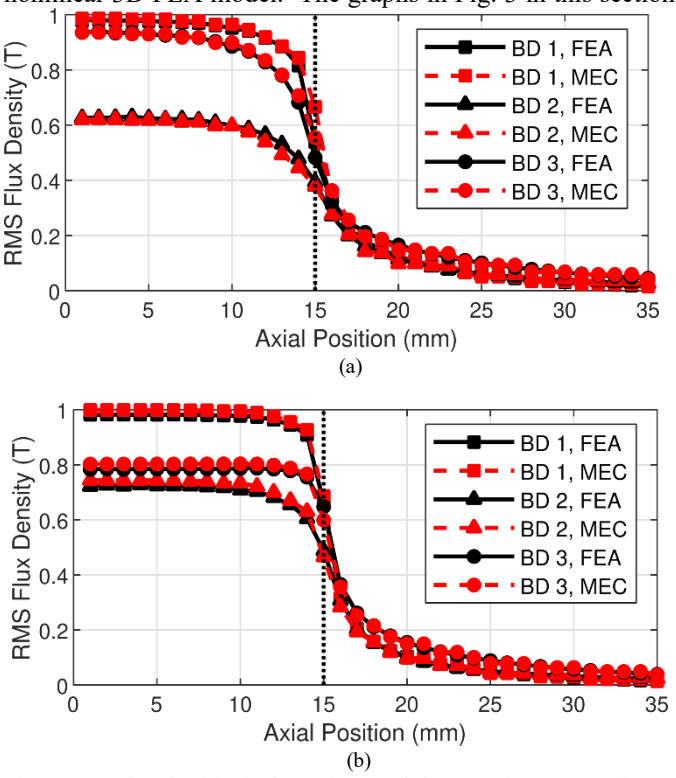

Fig. 3. RMS flux densities in the (a) inner and (b) outer air gaps according to 3D FEA and the 3D MEC models for each base design with a 30 mm stack length. The axial position is the axial distance from the middle of the gear. The dotted lines at 15 mm indicate the axial ends of the gears in the symmetrical half stack length models.

provide a comparison of the linear 3D MEC and nonlinear 3D FEA models' flux density predictions in the inner and outer air gaps at different axial positions, both within and axially beyond the gear. These graphs illustrate the MEC's ability to accurately capture the variations in flux density associated with axial position. The MEC model general predicts slightly higher flux density values than the FEA model and this is likely a result of the fact that the MEC model does not account for saturation in the ferromagnetic material. For these graphs, the MEC employed the cross-sectional mesh settings from Table II and N_{LIG} = 12, $k_{z,IG}$ = 2, N_{LOG} = 12, and $k_{z,OG}$ = 2.5. The dotted lines in the graphs in Fig. 3 indicate the axial ends of the gears in the symmetrical half stack length models.

IV. Axial Stack Length Sweeps

Next, to demonstrate the 3D MEC model's ability to track the variation of 3D effects with different axial stack lengths, the three base designs were evaluated using both the 3D MEC model and an ANSYS Maxwell 3D FEA model at stack lengths in the range of 20 mm to 150 mm in 10 mm steps and stack lengths in the range of 175 mm to 500 mm in 25 mm steps. Based on the results of the axial discretization parameters sweep study, the fixed axial discretization settings N_{LIG} = 3, $k_{z,IG}$ = 2, N_{LOG} = 10, and $k_{z,OG}$ = 2.5 were selected for use in this analysis. Additionally, the base designs were also analyzed by using an ANSYS Maxwell 2D FEA model and scaling the results to the appropriate stack lengths for comparison with the 3D model torque predictions.

Fig. 4 shows the LSR slip torque predicted by each of the different models for each of the different base designs at all of the evaluated axial stack lengths. Fig. 5 displays the same information for a subset of the shorter stack lengths, where 3D effects are more significant, to provide a better perspective of the relative accuracies of the different models. Fig. 6 provides the volumetric torque densities (VTDs) of the points displayed in Fig. 4. These results demonstrate that the 3D MEC model is extremely accurate, relative to the 3D FEA model, and capable of tracking the change in slip torque of a given cross-sectional design over a wide range of axial stack lengths. Notably, the 3D MEC model is very accurate even at short stack lengths, which suffer from the most significant 3D effects. In contrast, Figs. 5 and 6 clearly reveal that the 2D FEA model significantly overestimates the gear torque ratings at short stack lengths. As the stack length of a magnetic gear design increases, the 3D MEC model remains extremely accurate; however, the 2D FEA model also becomes increasingly accurate. The graphs in Fig. 4-6 demonstrate that

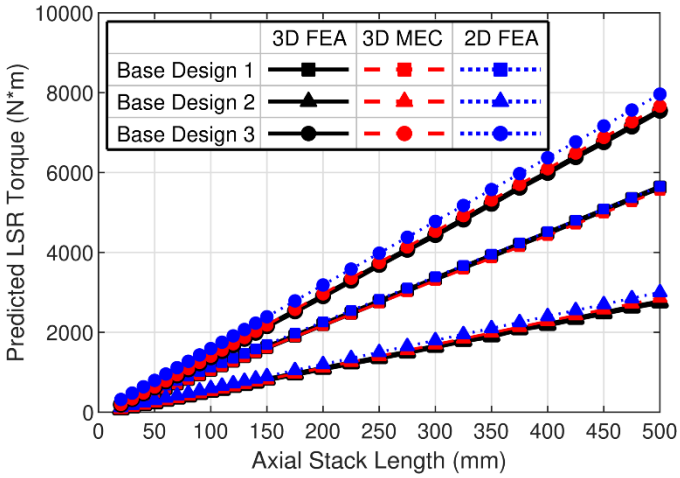

Fig. 4. Base design LSR slip torque predictions by the 3D FEA, 3D MEC, and 2D FEA models for all evaluated stack lengths.

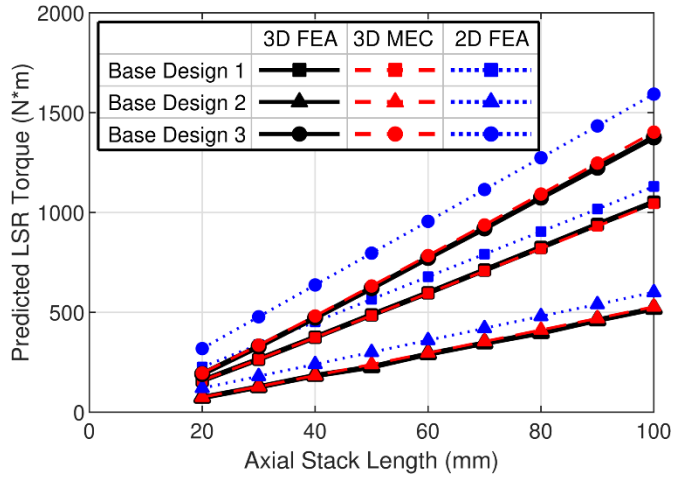

Fig. 5. Base design LSR slip torque predictions by the 3D FEA, 3D MEC, and 2D FEA models for a subset of shorter stack lengths.

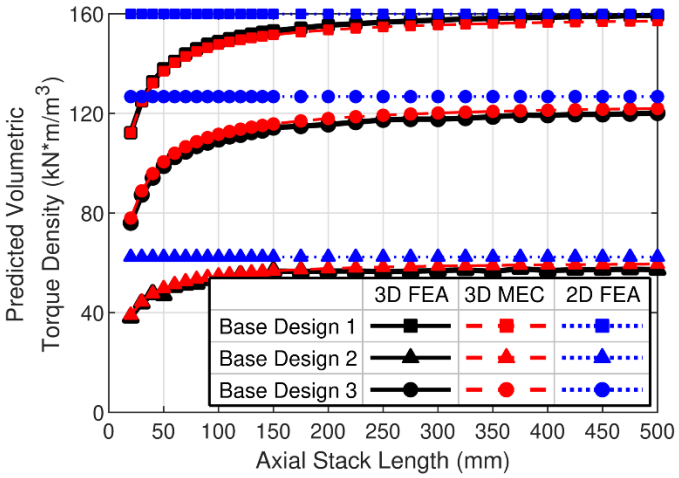

Fig. 6. Base design volumetric torque density predictions by the 3D FEA, 3D MEC, and 2D FEA models for all evaluated stack lengths.

as the stack length of a gear increases, the 2D FEA model still overestimates the torque rating; however, the difference simply becomes less significant as the gear torque rating grows with the stack length.

Although the VTDs shown in Fig. 6 effectively provide the same information as the results in Figs. 4 and 5, VTD provides an inherent scaling to better illustrate the changes in the relative accuracies of the different models with stack length. The 3D MEC model VTD predictions consistently match the 3D FEA model predictions within a few percent across the full range of evaluated axial stack lengths, but the 2D FEA model significantly overestimates the VTD of each design by as much as 67% at the shorter stack lengths and gradually becomes more accurate as the stack length increases and the relative significances of the end effects diminish.

Not only is the 3D MEC model an accurate analysis tool, as demonstrated by the results in Figs. 4-6, but it is also an extremely fast analysis tool. The preceding axial stack length sweep study consisted of 28 different stack lengths for 3 different base designs, resulting in a total of 84 different simulation cases. The 3D FEA simulations of these 84 cases took a total of 1 day, 17 hours, 8 minutes and 9 seconds. In contrast, the 3D MEC simulations of these 84 cases took a mere total of 7 minutes and 59 seconds, with an average torque prediction difference of 1.2% and an average absolute torque prediction discrepancy of 1.8% relative to the corresponding torque predictions of the nonlinear 3D FEA model. Thus, for the conditions used in this study, the 3D MEC model was approximately 309 times faster than the 3D FEA model on average. As noted in the discussion of the 2D MEC simulation speed [9], the simulation times required for the MEC and FEA models depend on a plethora of different considerations, including the designs evaluated, the model settings, and the computers used in the analysis. This timing data is simply intended to provide a general indication of the relative speeds of the different models, rather than exact characterizations. A strict convergence criterion was used for the FEA model employed in this analysis to ensure extremely accurate results and a reliable set of reference data for comparison against the MEC model predictions. A looser convergence setting could be used for the FEA model to make it faster, but this would also introduce more error into its torque predictions. Similarly, as previously mentioned, the 3D MEC model accuracy could be improved even more by using higher resolution discretization settings, but that would also result in slower simulation times.

Finally, when comparing the relative simulation speeds of the 3D MEC and 3D FEA models, it is also important to note that the MEC model used in this analysis employed a fixed number of axial layers; therefore, its simulation run time was invariant with respect to stack length. In contrast, the 3D FEA model's simulation time increased significantly with respect to stack length. In light of this consideration, it is clear that including large stack lengths of up to 500 mm biased the simulation times in favor of the MEC model. Furthermore, based on the results in Figs. 4-6, a 3D model is not nearly as essential at the larger stack lengths as it is at the shorter stack lengths. However, even if the timing comparison is limited to only the 27 simulation cases with stack lengths of 100 mm or less, for which 3D models are generally more necessary, then the 3D MEC model was still 109 times faster than the 3D FEA model on average. Regardless of these details, the 3D MEC model is undoubtedly an extremely fast and accurate analysis tool with potential advantages over standard commercial FEA models in certain situations.

V. Optimization Study

As in [9], a parametric optimization study was performed to validate the 3D MEC's utility as a quick optimization tool. Table IV describes the parametric sweep values used in this optimization study. As in [9], derived parameters were used in Table IV to avoid undesirable design scenarios. G_{Int} represents the integer portion of the gear ratio and relates the pole pair counts according to

$$P_{LS} = \begin{cases} G_{Int}P_{HS} + 1 & \text{for } (G_{Int}+1)P_{HS} \text{ odd} \\ G_{Int}P_{HS} + 2 & \text{for } (G_{Int}+1)P_{HS} \text{ even} \end{cases}. \quad (5)$$

This relationship avoids designs with integer gear ratios, which tend to have high torque ripple, and designs without any periodic symmetry in a cross-section, which have unbalanced magnetic forces on the rotors. The radial thicknesses of the two sets of magnets are related by k_{PM} according to

$$T_{LSPM} = k_{PM} T_{HSPM}. \quad (6)$$

As described in [7], due to leakage flux, it is generally optimal to have thicker magnets on the HSR than on the LSR. Finally, to avoid excessive saturation in the HSR back iron, its radial thickness is related to the HSR pole arc by k_{HSBI} according to

$$T_{HSBI} = k_{HSBI}(\pi r_{HSBI}/P_{HS}). \quad (7)$$

Both ANSYS Maxwell, a commercial FEA software, and the 3D MEC model were used to evaluate the torque of each of the 144,342 designs specified in Table IV. The MEC used the cross-sectional discretization parameter values listed in Table II and the axial discretization settings employed in the previous section. Due to symmetry, only half of the gear stack length was used in both the 3D FEA and 3D MEC models.

TABLE IV
Optimization Study Parameter Sweep Values

Parameter	Description	Ranges of Values	Units
G_{Int}	Integer part of gear ratio	4, 8, 16	
P_{HS}	HSR pole pairs		
	For $G_r = 4$	3, 4, 5, … 18	
	For $G_r = 8$	3, 4, 5, … 13	
	For $G_r = 16$	3, 4, 5, … 8	
r_{out}	Active outer radius	150, 175, 200	mm
k_{HSBI}	HSR back iron thickness coefficient	0.4, 0.5, 0.6	
T_{HSPM}	HSR magnet thickness	3, 5, 7, … 13	mm
T_{AG}	Common air gap thickness	1.5	mm
T_{Mods}	Modulator thickness	11, 14, 17	mm
k_{PM}	LSR magnet thickness ratio	0.5, 0.75, 1	
T_{LSBI}	LSR back iron thickness	20, 25, 30	mm
L_{Stack}	Axial stack length	30, 100, 300	mm

The graphs in Figs. 7-10 and the statistics in Table V show the comparison between the results for the 3D MEC, 2D FEA, and 3D FEA models. Fig. 7 shows that, while the 2D FEA model tends to overestimate the designs' torques, especially at short stack lengths, the 3D MEC model matches the 3D FEA model much more consistently. Additionally, Fig. 7(a) illustrates that the 3D MEC model agrees best with the 3D FEA model for the designs with the highest VTD, while the most significant disagreements occur for designs with lower VTDs than the optimal designs. Some of the mismatch in torque predictions is due to the 3D FEA. For a few of the cases with the worst matches, the 3D FEA model was run with a tighter energy error convergence criterion, which resulted in a change in torque of up to 4% for one case. However, it would be computationally impractical to run all 144,342 cases with such a tight convergence criterion. Also, the 3D FEA simulations for this parametric sweep were run across multiple computing clusters to facilitate their completion in a reasonable amount of time; however, this means that any comparison of the simulation timing data for the different models would be very inconsistent.

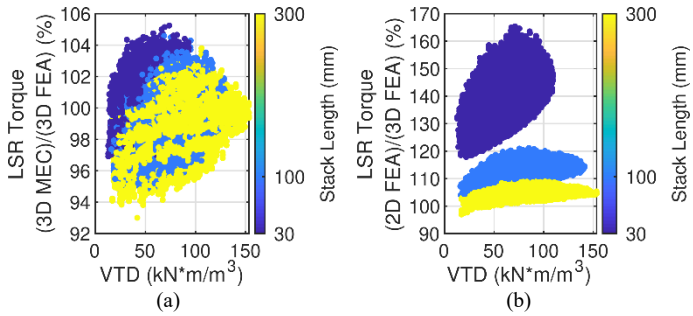

Fig. 7. LSR torque prediction agreements between (a) the 3D MEC and 3D FEA models and (b) the 2D FEA and 3D FEA models.

TABLE V
Comparison of LSR Torque Predictions Relative to 3D FEA

Model	3D MEC			2D FEA		
Stack Length	30 mm	100 mm	300 mm	30 mm	100 mm	300 mm
Minimum Difference	-4.6%	-5.5%	-7.0%	17.9%	2.7%	-3.1%
Maximum Difference	5.2%	4.6%	3.8%	65.4%	21.1%	9.0%
Average Difference	0.5%	-0.2%	-0.6%	35.5%	10.6%	3.5%
Average Absolute Discrepancy	0.8%	0.8%	1.0%	35.5%	10.6%	3.5%

Figs. 8 – 10 illustrate that the MEC is able to accurately track the performance trends associated with key parameters. The 3D MEC accurately predicts trends in VTD and PM VTD, which is the LSR slip torque divided by the volume of the PMs. Figs. 8 – 10 also show that, while the 2D FEA model exhibits significant error in predicting VTD and PM VTD for designs with short stack lengths, 2D FEA does accurately predict which values of key parameters are optimal. For this study, all designs had the same set of stack lengths. However, if the stack length was adjusted for each design to meet a target slip torque, then including 3D effects in the analysis would affect the optimal parameter values [7]. Thus, while 2D FEA or 2D MEC models may be appropriate for a rapid initial optimization, the 3D MEC provides a means for more accurate analysis that can still be faster than 3D FEA.

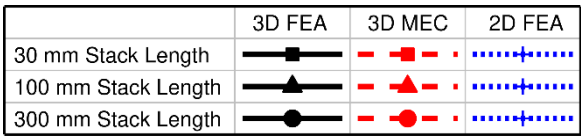

Fig. 8. Legend for Figs. 9 and 10.

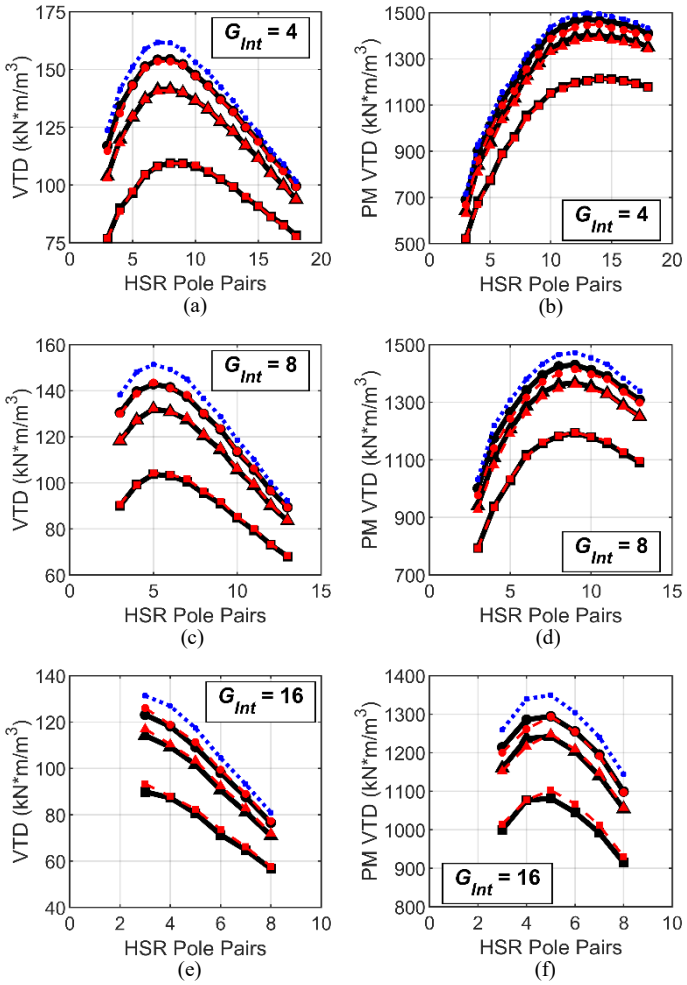

Fig. 9. Variation of the maximum achievable (a), (c), (e) volumetric torque density and (b), (d), (f) PM volumetric torque density with HSR pole pairs for designs with $G_{Int} = 4$, $G_{Int} = 8$, and $G_{Int} = 16$.

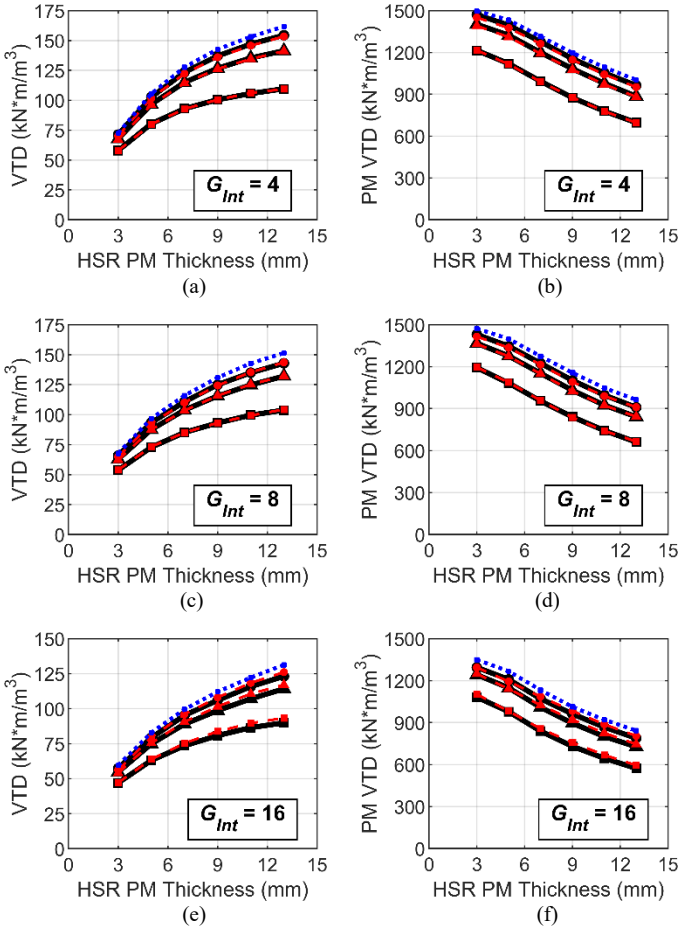

Fig. 10. Variation of the maximum achievable (a), (c), (e) volumetric torque density and (b), (d), (f) PM volumetric torque density with HSR magnet thickness for designs with $G_{Int} = 4$, $G_{Int} = 8$, and $G_{Int} = 16$.

VI. Conclusions

This is Part II of a two-part paper on a parameterized linear 3D MEC for radial flux magnetic gears with surface permanent magnets. Part I explains the systematic implementation of the 3D MEC model. This section develops guidelines for the model's axial discretization and compares it against 2D FEA and 3D FEA models to evaluate its accuracy. Because 2D FEA significantly overpredicts the slip torque of designs with short stack lengths, a 3D model is required. The 3D MEC agrees well with the 3D FEA model, exhibiting an average absolute discrepancy of less than 1% for a parametric study with 144,000 cases. However, the 3D MEC can evaluate the designs much faster than the 3D FEA model.

It is important to note that this implementation of the 3D MEC model approximates the ferromagnetic material as linear with constant permeability and design scenarios with thin components may experience significant saturation that will not be accurately characterized by this model, as described for the 2D MEC in [9]. Future work on this subject will include the development of a nonlinear MEC model variation employing B-H curve characteristics and the application of the MEC model to other magnetic gear and electric machine topologies. The use of a nonlinear B-H curve will be critical for modeling designs with thin modulators or back irons and characterizing the impact of modulator retention features, such as the bridge between adjacent modulators used in [1], [3]-[6].

VII. References

[1] S. Gerber and R-J. Wang, "Analysis of the End-Effects in Magnetic Gears and Magnetically Geared Machines," in *Proc. IEEE Int. Conf. Elect. Mach.*, 2014, pp. 396-402.

[2] M. Johnson, M. C. Gardner, and H. A. Toliyat, "Design Comparison of NdFeB and Ferrite Radial Flux Surface Permanent Magnet Coaxial Magnetic Gears," *IEEE Trans. Ind. Appl.*, vol. 54, no. 2, pp. 1254-1263, Mar.-Apr. 2018.

[3] H. Y. Wong, J. Z. Bird, D. Barnett and W. Williams, "A High Torque Density Halbach Rotor Coaxial Magnetic Gear," in *Proc IEEE Int. Elect. Mach. Drives Conf.*, 2019, pp. 233-239.

[4] K. Li, S. Modaresahmadi, W. B. Williams, J. Z. Bird, J. D. Wright, and D. Barnett, "Electromagnetic Analysis and Experimental Testing of a Flux Focusing Wind Turbine Magnetic Gearbox," *IEEE Trans. Energy Convers*, vol. 34, no. 3, pp. 1512-1521, Sept. 2019.

[5] S. Gerber and R.-J. Wang, "Evaluation of a Prototype Magnetic Gear," in *Proc. IEEE Int. Conf. Ind. Technol.*, 2013, pp. 319-324.

[6] T. V. Frandsen and P. O. Rasmussen, "Slip Torque Investigation and Magnetic Redesign of Motor Integrated Permanent Magnet Gear," in *Proc. Int. Conf. Elect. Mach. Syst.*, 2015, pp. 929-935.

[7] M. C. Gardner, B. E. Jack, M. Johnson, and H. A. Toliyat, "Comparison of Coaxial Radial Flux Magnetic Gears Independently Optimized for Volume, Cost, and Mass," *IEEE Trans. Ind. Appl.*, vol. 54, no. 3, pp. 2237-2245, May/June 2018.

[8] M. Johnson, M. C. Gardner and H. A. Toliyat, "A Parameterized Linear Magnetic Equivalent Circuit for Analysis and Design of Radial Flux Magnetic Gears—Part I: Implementation," *IEEE Trans. Energy Convers.*, vol. 33, no. 2, pp. 784-791, June 2018.

[9] M. Johnson, M. C. Gardner and H. A. Toliyat, "A Parameterized Linear Magnetic Equivalent Circuit for Analysis and Design of Radial Flux Magnetic Gears—Part II: Evaluation," *IEEE Trans. Energy Convers.*, vol. 33, no. 2, pp. 792-800, June 2018.

VIII. Biographies

Matthew Johnson (S' 13, M'17) earned his B.S. and Ph.D. both in electrical engineering from Texas A&M University, College Station, Texas, in 2011 and 2017, respectively. He is currently an electronics engineer for the U.S. Army Research Laboratory. His research interests include the design and control of electric machines and magnetic gears.

Matthew C. Gardner (S'15, M'19) earned his B.S. in electrical engineering from Baylor University, Waco, Texas in 2014. He earned his Ph.D. in electrical engineering from Texas A&M University, College Station, Texas in 2019. In August 2020, he joined the University of Texas at Dallas, where he is an assistant professor. His research interests include optimal design and control of electric machines and magnetic gears.

Hamid A. Toliyat (S'87, M'91, SM'96, F'08) received the B.S, degree from Sharif University of Technology, Tehran, Iran in 1982, the M.S. degree from West Virginia University, Morgantown, WV in 1986, and the Ph.D. degree from University of Wisconsin-Madison, Madison, WI in 1991, all in electrical engineering. In March 1994 he joined the Department of Electrical and Computer Engineering, Texas A&M University where he is currently the Raytheon endowed professor of electrical engineering. Dr. Toliyat has many papers and awards to his name, including the Nikola Tesla Field Award.